THE JOURNAL OF PHYSICAL CHEMISTRY A

Article

pubs.acs.org/JPCA

Ab Initio Unimolecular Reaction Kinetics of $CH_2C(=O)OCH_3$ and $CH_3C(=O)OCH_2$ Radicals

Ting Tan,[†] Xueliang Yang,[‡] Yiguang Ju,[‡] and Emily A. Carter*[,‡,§,∥]

[†]Department of Chemistry, [‡]Department of Mechanical and Aerospace Engineering, [§]Program in Applied and Computational Mathematics, and [∥]Andlinger Center for Energy and the Environment, Princeton University, Princeton, New Jersey 08544, United States

Supporting Information

ABSTRACT: The unimolecular dissociation and isomerization kinetics of the methyl ester combustion intermediates methoxycarbonylmethyl ($CH_2C(=O)OCH_3$) and acetyloxylmethyl ($CH_3C(=O)OCH_2$) are theoretically investigated using high-level ab initio methods and the Rice−Ramsperger−Kassel−Marcus (RRKM)/master equation (ME) theory. Potential energy surfaces (PESs) are obtained using coupled cluster singles and doubles with perturbative triples correction (CCSD(T)), multireference singles and doubles configuration interaction (MRSDCI) with the Davidson−Silver (DS) correction, and multireference averaged coupled pair functional (MRACPF2) theory. The transition states exhibit high T1 diagnostics in coupled cluster calculations, suggesting the need for a multireference correlated wave function treatment. MRSDCI+DS and MRACPF2 capture their multiconfigurational character well, yielding lower barrier heights than CCSD(T) for these reactions. The rate coefficients are computed using the RRKM/ME theory over a 500−2500 K temperature range and at a pressure range of 0.01 atm to the high-pressure limit. The temperature- and pressure-dependent rate coefficients are given in modified Arrhenius expressions. The β-scission of $CH_2C(=O)OCH_3$ is predicted to have a much higher barrier than the corresponding isomerization reaction and the β-scission of $CH_3C(=O)OCH_2$. Consequently, the rate coefficients for β-scission of $CH_2C(=O)OCH_3$ are the smallest among the three reactions and the isomerization followed by decomposition to $CH_3C(=O)$ and HCHO is the dominant reaction pathway for $CH_2C(=O)OCH_3$. Both radicals $CH_2C(=O)OCH_3$ and $CH_3C(=O)OCH_2$ are predicted to mainly decompose to $CH_3C(=O)$ + HCHO rather than to the bimolecular product $CH_2C(=O)$ + CH_3O. A newly developed MA combustion mechanism, using our theoretical rate coefficients for the MA-related reactions, predicts combustion properties in good agreement with available experimental data.

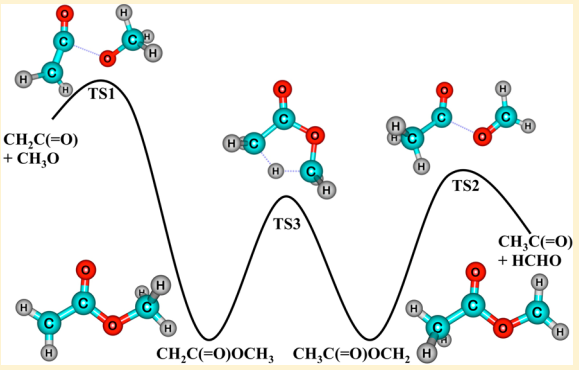

1. INTRODUCTION

Enormous problems arise from our use of fossil fuels, such as global climate change and energy insecurity and unsustainability, leading to an increasing call for renewable energy sources. Among the alternatives to fossil fuels, biodiesel has attracted significant interest, especially in the transportation sector. The physical properties of biodiesel are similar to those of petroleum diesel, but utilization of biodiesel has the potential to reduce emissions of particulate matter, CO, and net CO_2, compared to using the corresponding fossil fuels.[1,2] Current biodiesels are mainly derived from transesterification of lipids to produce long-chain fatty acid methyl esters.[3] The combustion properties of these oxygenated fuels are distinct from conventional hydrocarbons, and therefore thorough investigations into combustion mechanisms are required before they can be reliably used in current engines. However, because of the large size of biodiesel molecules, smaller methyl esters are often utilized as surrogates both experimentally and theoretically. These surrogates contain the same methyl ester functional group but a relatively short alkyl chain that possesses kinetics properties similar to those of intermediates in biodiesel oxidation.[3,4] Systematic investigations of these small surrogates aid our understanding of the oxidation mechanisms for actual biodiesels and also provide insights into the differences and similarities that biodiesels have with the corresponding fossil fuels.

As the simplest methyl ester with an alkyl side chain, the oxidation kinetics of methyl acetate (MA, $CH_3C(=O)OCH_3$) has been experimentally and theoretically studied fairly extensively.[5−12] MA is mainly consumed by H-abstraction under most combustion conditions, resulting in two distinct MA radicals, methoxycarbonylmethyl ($CH_2C(=O)OCH_3$) and acetyloxylmethyl ($CH_3C(=O)OCH_2$).[5,7,11] These two radicals may either directly break down through β-scission reactions or isomerize to the other via an intramolecular H atom transfer, as follows:

Received: August 27, 2015
Revised: October 3, 2015

ACS Publications © XXXX American Chemical Society

DOI: 10.1021/acs.jpca.5b08331
J. Phys. Chem. A XXXX, XXX, XXX−XXX

$$CH_2C(=O)OCH_3 \rightarrow CH_2C(=O) + CH_3O \quad (R1)$$

$$CH_3C(=O)OCH_2 \rightarrow CH_3C(=O) + HCHO \quad (R2)$$

$$CH_2C(=O)OCH_3 \rightarrow CH_3C(=O)OCH_2 \quad (R3)$$

Two pairs of bimolecular products may be formed: ketene ($CH_2C(=O)$) and methoxy radical (CH_3O), as well as acetyl radical ($CH_3C(=O)$) and formaldehyde (HCHO). These products may then further decompose/react with other species to form the final products of combustion. Rate coefficients of the MA-specific reactions, such as MA H-abstraction and unimolecular reactions of the MA radicals, have a large impact on its correspondingly distinct combustion properties. Therefore, knowledge of accurate rate coefficients is crucial to understanding MA combustion chemistry.

To date, a few MA combustion mechanisms have been developed mainly on the basis of structural similarities between MA and other species, and many kinetics parameters have been estimated, especially for the MA-specific reactions.[5,8,10] For example, the high-pressure-limit rate coefficients for reactions R1 and R2 in Dagaut et al.'s MA mechanism[5] were assumed to be the same as the decomposition of i-$C_4H_7 \rightarrow C_3H_4 + CH_3$ and $CH_3OCH_2 \rightarrow CH_3 + HCHO$, respectively. Westbrook et al.[10] estimated high-pressure-limit rate constants for the reverse of reactions R1 and R2 in their MA combustion model, which were then used in an updated MA pyrolysis mechanism by Peukert et al.[8] These diverse estimates suggest a crucial need for more accurate rate coefficients.

Huynh and Violi[13] theoretically studied the β-scission reaction of $CH_2C(=O)OCH_3$ (reaction R1) at the density functional theory (DFT)[14]-BH&HLYP/cc-pVTZ level and utilized Rice−Ramsperger−Kassel−Marcus (RRKM)[15−17] theory to compute its high-pressure-limit rate constants, which were then utilized in their methyl butanoate oxidation model. No calculations or experiments for the high-pressure-limit rate coefficients of reactions R2 and R3 have been reported, to the best of our knowledge. Moreover, the unimolecular decomposition reaction rates are both temperature- and pressure-dependent. Incorporating pressure-dependence into kinetics models is necessary to properly descibe the kinetics properties at various conditions, especially at relatively high temperatures. Pressure-dependent rate constants for Ri (i = 1−3) were implemented in a recently published methyl propanoate oxidation model by Zhao et al.,[18] but only within a small pressure range of 0.006−2.0 atm. Because most combustion devices operate at much higher pressures, kinetics parameters for high pressures are needed for the development of robust combustion models.

Motivated by the above disscussions, the decomposition and isomerization reactions of $CH_2C(=O)OCH_3$ and $CH_3C(=O)OCH_2$ are theoretically investigated in this work. Both temperature- and pressure-dependent rate constants are computed and reported in modified Arrhenius expressions. DFT[14] is applied to locate the stationary points along the reaction pathways. The energies at stationary points are refined via coupled-cluster singles and doubles with perturbative triples correction (CCSD(T)),[19] multireference singles and doubles configuration interaction (MRSDCI)[20] with Davidson−Silver (DS)[21] size-extensivity corrections, and multireference averaged coupled pair functional (MRACPF2)[22,23] theory. Rate coefficients are computed using RRKM[15−17] theory with the master equation (ME)[24,25] approach in the temperature range of 500−2500 K and the pressure range of 0.01 atm to the high-pressure limit.

2. COMPUTATIONAL METHODS AND DETAILS

All geometry optimizations were performed using DFT and the M08-HX[26] hybrid exchange-correlation functional with the cc-pVTZ[27] basis set in the GAMESS-US[28] program package. Unrestricted DFT was used for open-shell radicals, while closed-shell molecules were described with restricted DFT. A transition state (TS) was confirmed first by verifying the presence of one single imaginary frequency as an eigenvalue of the numerical Hessian matrix (constructed from finite differences of analytic gradients) and then by an intrinsic reaction coordinate analysis at the DFT-M08-HX/cc-pVDZ level to verify the TS's connection to the corresponding reactant and product. Harmonic vibrational frequencies and zero-point energies (ZPEs) were obtained within the harmonic oscillator approximation and scaled by a factor of 0.974.[29]

Energies of all critical points on the potential energy surface (PES) were refined using CCSD(T) with basis sets cc-pVXZ (X = D, T, Q)[27] in the MOLPRO[30] code. To examine the multiconfigurational character of these reactions, we used MRSDCI with the DS correction as well as MRACPF2 to obtain stationary point energies within the MOLCAS[31] and TIGERCI[32−40] codes with basis sets cc-pVXZ (X = D, T). A supermolecule scheme with two fragments 10 Å apart was used to ensure size-consistency in the multireference methods when determining energies of dissociated products. At each critical point, a consistent CAS(7e, 7o), i.e., seven electrons in seven active orbitals, was used as the active space in complete active space self-consistent field (CASSCF) calculations. It included the bonding and antibonding orbitals of the breaking C−O and C−H bonds respectively involved in decomposition and isomerization reactions, C=O π and π* orbitals, and singly occupied orbitals, as well as the corresponding electrons. All configuration state functions in the CASSCF wave function with coefficients larger than 0.01 were then used as references in the MRSDCI+DS and MRACPF2 calculations. A Cholesky decomposition scheme with a threshold of 1.0×10^{-7} was employed to efficiently evaluate the two-electron integrals. The frozen-core approximation was applied for all three methods. The complete basis set (CBS) limit E_∞ was then obtained using the two-point extrapolation scheme[41] given by

$$E(l_{max}) = E_\infty + \frac{B}{(l_{max} + 1)^4}$$

where l_{max} is the maximum angular momentum function found within the basis sets, and B is a system-specific parameter.

Using the computed energetics and molecular properties described above, we then predicted the temperature- and pressure-dependent rate constants using RRKM theory and the multiwell one-dimensional (1D) ME approach in the VARIFLEX[42] code. The rates were investigated at total internal energy (E) and total angular momentum quantum number (J) resolved levels. The translational, rotational, and vibrational partition functions were all obtained at the DFT-M08-HX/cc-pVTZ level within the ideal gas, rigid rotor, and harmonic oscillator approximations, respectively. We treated the torsional rotations along a single bond within the 1D separable-hindered rotor approximation, which is a sufficiently accurate description of these degrees of freedom. As described in our previous work,[12,43] a relaxed scan was performed to obtain the torsional

DOI: 10.1021/acs.jpca.5b08331
J. Phys. Chem. A XXXX, XXX, XXX−XXX

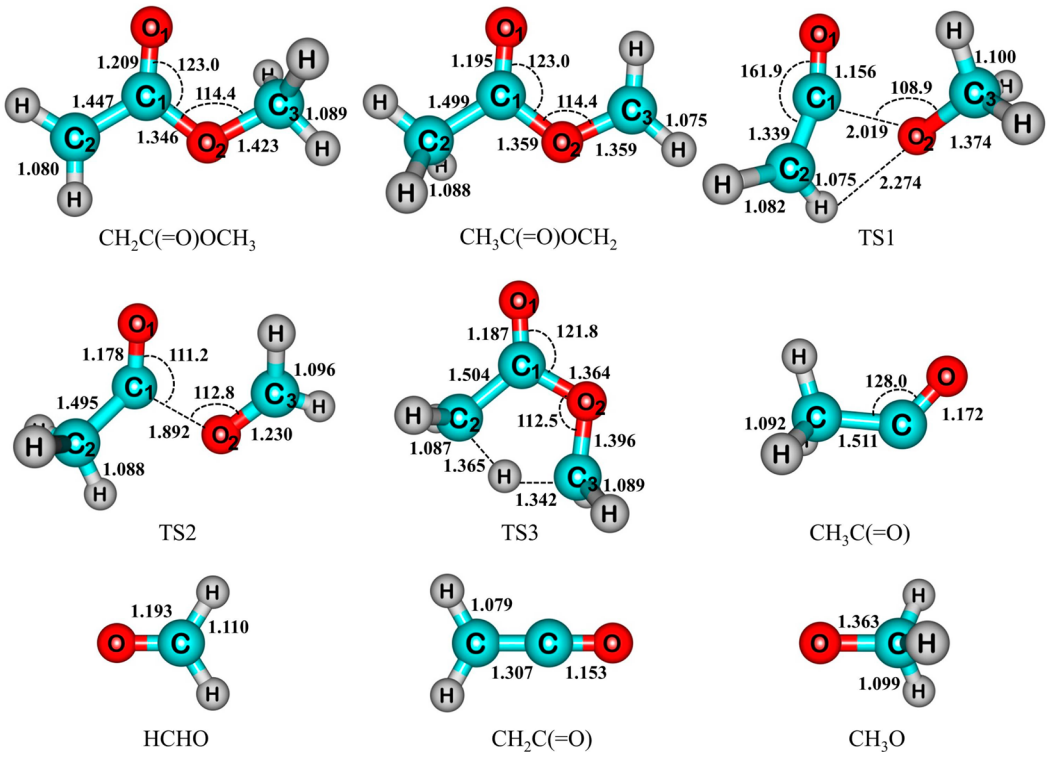

Figure 1. DFT-M08-HX/cc-pVTZ optimized geometries of $CH_2C(=O)OCH_3$, $CH_3C(=O)OCH_2$, and corresponding transition states (TSs) and products of the dissociation and isomerization reactions. Bond lengths are given in ångstroms and angles in degrees.

PES for the equilibrium structure whereas we additionally froze the lengths of the breaking and forming bonds for the TS. Nitrogen (N_2) or argon (Ar) was assumed as the bath gas. The results using the bath gas N_2 are reported in this work, and the corresponding results with Ar as the bath gas are additionally provided in the Supporting Information. The Lennard-Jones (LJ) collision diameter parameter σ for N_2 is 3.798 Å and the well-depth ε is 49.6 cm^{-1}.[44] We used the exponential-down model for energy transfer coefficients with the average downward transfer parameter $\langle \Delta E \rangle_{down} = 400(T/298\ K)^{0.8}$ cm^{-1}. The LJ parameters for $CH_2C(=O)OCH_3$ and $CH_3C(=O)OCH_2$ were taken to be the same as MA, which were σ = 4.936 Å and ε = 326.5 cm^{-1}.[44] The ME calculations were performed in the temperature range of 500−2500 K and pressure range of 0.01−100 atm. The tunneling effect was approximated using the asymmetric Eckart approximation.[45]

3. RESULTS AND DISCUSSION

Structural and energetic features are discussed in section 3.1, followed by a presentation of reaction kinetics in section 3.2. The TS of each reaction R*i* (i = 1−3) is referred to as TS*i* (*i* = 1−3), respectively. Complete structural information and frequencies for all species are provided in the Supporting Information.

3.1. Potential Energy Surface. Figure 1 compares the optimized geometries of all critical points on the PES obtained at the DFT-M08-HX/cc-pVTZ level. The carbon atom at the radical site of $CH_2C(=O)OCH_3$ or $CH_3C(=O)OCH_2$ is sp^2 hybridized, resulting in an extended π-resonance structure with the C=O π orbital. The direct resonance involving the C1−C2 bond in $CH_2C(=O)OCH_3$ is therefore 0.052 Å shorter than the counterpart in $CH_3C(=O)OCH_2$, whereas the bond lengths of C1−O2 are 1.346 and 1.359 Å for $CH_2C(=O)OCH_3$ and $CH_3C(=O)OCH_2$, respectively, because of the less effective π-resonance via the methoxy O 2pπ. Both reactions R1 and R2 involve cleavage of the C1−O2 bond. The C1−O2 bond of TS1 is elongated by ∼57% compared with the reactant, and the bond length of C1−C2 is reduced to 1.339 Å from 1.447 Å due to the partly formed C1−C2 π bond in the incipient ketene molecule. This indicates a late TS, as is expected for an endothermic reaction. Likewise, the C1−O2 bond of TS2 is also stretched by ∼39% relative to that in $CH_3C(=O)OCH_2$, which is less than in TS1. The intramolecular H atom transfer for the isomerization reaction R3 proceeds via a planar ring structure, and the dihedral angle of C2C1O2C3 of TS3 changes substantially to 0.0° from 179.8°, compared to the reactant. The transferring H atom in TS3 is 1.365 and 1.342 Å away from C2 and C3, respectively.

The PES for this reaction system is depicted in Figure 2, in which energies of all stationary points are relative to the $CH_2C(=O)OCH_3$ energy with ZPE correction. The energies refined by CCSD(T) are computed with the cc-pV*X*Z (*X* = D, T, Q) basis sets. The two-point extrapolation to the CBS limit using energies obtained with cc-pV*X*Z (*X* = D, T) is labeled as CBS(D-T), and similarly, CBS(T-Q) is the extrapolation from the cc-pV*X*Z (*X* = T, Q) basis sets. The mean unsigned deviation between the two extrapolations at the CCSD(T) level is only 0.55 kcal/mol. Given this good accuracy of CBS(D-T) compared to CBS(T-Q), we only extrapolate our results at the D-T level to reduce computational cost for the more expensive multireference methods (vide infra).

For CCSD(T) calculations, the T1 diagnostic is often used to estimate the expected importance of multiconfigurational character. A T1 diagnostic of <0.02 for a closed-shell molecule[46] and a T1 diagnostic of <0.04 for a radical[47] were suggested as bounds for a reliable single-reference calculation. Some species in this reaction system have relatively large T1

DOI: 10.1021/acs.jpca.5b08331
J. Phys. Chem. A XXXX, XXX, XXX−XXX

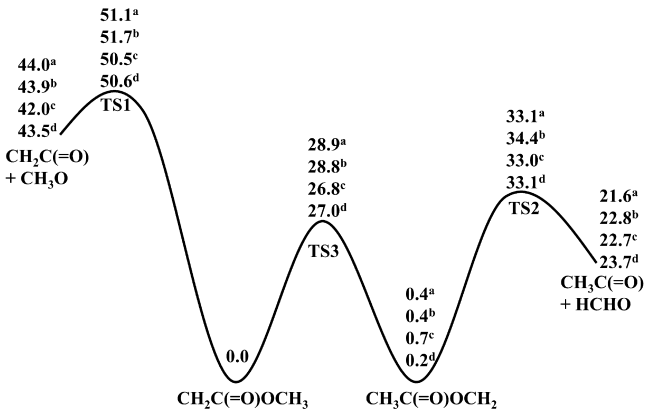

Figure 2. ZPE-corrected PES for dissociation and isomerization reactions of $CH_2C(=O)OCH_3$ and $CH_3C(=O)OCH_2$. The geometries are optimized at the DFT-M08-HX/cc-pVTZ level. The energies (kcal/mol) are refined at four levels: (a) CCSD(T)/CBS(T-Q); (b) CCSD(T)/CBS(D-T); (c) MRACPF2/CBS(D-T); and (d) MRSDCI+DS/CBS(D-T).

diagnostics, e.g., the T1 diagnostic for TS1 is ~0.07, indicating a significant multiconfigurational character. Thus, we apply the multireference based methods (MRSDCI+DS and MRACPF2) to ensure a physically accurate description for these species and also apply the same methods to the other critical points for consistency. Comparing the two multireference based methods, the relative TS energies predicted by MRSDCI+DS are only 0.1−0.2 kcal/mol higher than the MRACPF2 energies. However, larger deviations in energies are observed in the relative product energies predicted by MRSDCI+DS and MRACPF2. For a stretched molecule, Szalay[48] also showed that the deviation of MRSDCI+DS energies from full CI energies varied far more significantly than that of MRACPF2 energies with increasing bond length. This may result in the relative energy of the dissociated product predicted by MRSDCI+DS being less reliable than the MRACPF2 energy. Consequently, compared to MRSDCI+DS, MRACPF2 is recommended and the MRACPF2 energy will be used in the following kinetics studies. However, compared to CCSD(T), both MRSDCI+DS and MRACPF2 predict lower barrier heights for all three reactions by up to 2.0 kcal/mol. This is probably due to the higher multiconfigurational character of TSs compared to the two initial radicals.

The Active Thermochemical Tables (ATcT) of Goos, Burcat, and Ruscic[49] contain the standard heat of formation at 0 K ($\Delta_f H^0_{0K}$) of all species in reaction R2. From this, we compute the reaction energy of reaction R2 to be 23.1 kcal/mol. The reaction energies of reaction R2 obtained at the CCSD(T), MRSDCI+DS, and MRACPF2//CBS(D-T) levels are 22.4, 22.0, and 23.5 kcal/mol, respectively, which are in excellent agreement with the result computed using the $\Delta_f H^0_{0K}$, given the reported ±1.9 kcal/mol uncertainty for $CH_3C(=O)OCH_2$. Comparing the energetics of these three reactions in Figure 2, the β-scission of $CH_2C(=O)OCH_3$ (R1) has a much higher activation energy than of reaction R2 or R3, and the barrier height of isomerization reaction R3 is the smallest among the three reactions. This indicates that the isomerization channel is strongly favored over the β-scission decomposition for $CH_2C(=O)OCH_3$.

3.2. Rate Constants. The temperature- and pressure-dependent rate coefficients were obtained by solving the 1D ME. The rate constants were computed in the temperature range of 500−2500 K at increments of 100 K and in a pressure range of 0.01 atm to the high-pressure limit with the bath gas N_2. The RRKM/ME was solved with molecular properties and energies obtained at the CCSD(T)/CBS(T-Q) and MRACPF2/CBS(D-T) //DFT-M08-HX levels. The fitted modified Arrhenius expressions with MRACPF2 energies for all studied reactions are summarized in Table 1, and equivalent parameters with CCSD(T) energies are given in the Supporting Information.

Table 1. Rate Coefficients for the Unimolecular Dissociation and Isomerization Reactions of $CH_2C(=O)OCH_3$ and $CH_3C(=O)OCH_2$ in Modified Arrhenius Form ($k = AT^n \exp[-E_a/(RT)]$), Obtained with MRACPF2/CBS(D-T)//M08-HX/cc-pVTZ Energies

pressure	A (s^{-1})	n	E_a (cal/mol)
R1: $CH_2C(=O)OCH_3 \rightarrow CH_2C(=O) + CH_3O$			
p = 7.6 Torr	6.57×10^{9}	−0.61	43204
p = 30 Torr	3.03×10^{18}	−2.88	46648
p = 1 atm	4.33×10^{33}	−6.56	55540
p = 10 atm	2.81×10^{35}	−6.61	58396
p = 100 atm	5.74×10^{31}	−5.17	58792
high-pressure limit	2.09×10^{16}	−0.45	52500
R2: $CH_3C(=O)OCH_2 \rightarrow CH_3C(=O) + HCHO$			
p = 7.6 Torr	5.11×10^{32}	−6.63	35883
p = 30 Torr	4.32×10^{34}	−7.00	38083
p = 1 atm	3.82×10^{32}	−6.02	39362
p = 10 atm	1.74×10^{28}	−4.55	38645
p = 100 atm	1.12×10^{22}	−2.62	36416
high-pressure limit	7.24×10^{13}	−0.18	32707
R3: $CH_2C(=O)OCH_3 \rightarrow CH_3C(=O)OCH_2$			
p = 7.6 Torr	6.17×10^{25}	−4.90	25290
p = 30 Torr	5.90×10^{26}	−4.99	26802
p = 1 atm	8.33×10^{28}	−5.19	30526
p = 10 atm	4.76×10^{26}	−4.29	31185
p = 100 atm	1.03×10^{21}	−2.48	29565
high-pressure limit	1.97×10^{9}	1.03	24273
R4: $CH_2C(=O)OCH_3 \rightarrow CH_3C(=O) + HCHO$			
p = 7.6 Torr	3.64×10^{36}	−7.76	38715
p = 30 Torr	3.29×10^{40}	−8.65	43051
p = 1 atm	1.70×10^{39}	−7.84	46418
p = 10 atm	1.93×10^{42}	−8.36	53576
p = 100 atm	2.83×10^{33}	−5.63	53255
R5: $CH_3C(=O)OCH_2 \rightarrow CH_2C(=O) + CH_3O$			
p = 7.6 Torr	5.19×10^{14}	−2.10	44410
p = 30 Torr	3.42×10^{22}	−4.13	47430
p = 1 atm	1.30×10^{38}	−7.91	57543
p = 10 atm	3.86×10^{39}	−7.84	62524
p = 100 atm	7.64×10^{32}	−5.56	63931

To simplify the problem, $CH_2C(=O) + CH_3O$ was assumed as reactants, and the dissociation to bimolecular products $CH_3C(=O) + HCHO$ was treated irreversibly as the "infinite sink." The reactants were assumed to be in thermal equilibrium with the bath gas throughout the course of the reaction. Using the microcanonical rate constants obtained with RRKM theory, the 1D ME was solved, giving a set of eigenvalues and eigenvectors. The three slowest modes with the last three smallest absolute eigenvalues described the "chemical" processes, referred to as chemically significant eigenvalues (CSEs). The other modes then represented the intermolecular energy transfer, which were the internal-energy relaxation

DOI: 10.1021/acs.jpca.5b08331
J. Phys. Chem. A XXXX, XXX, XXX−XXX

eigenvalues (IEREs). The eigenvalue spectrum with MRACPF2 energies is plotted in Figure 3 at a pressure of 1 atm, where the

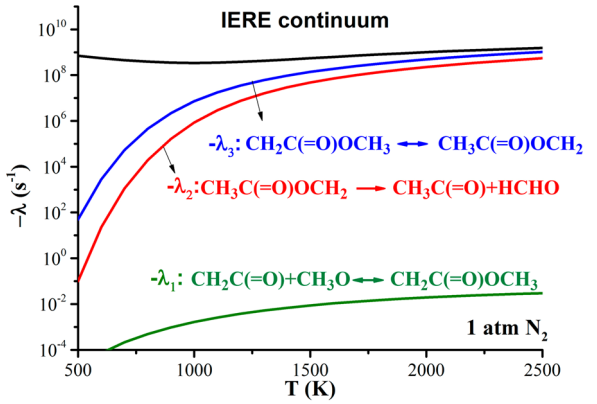

Figure 3. Eigenvalue spectrum ($-\lambda$) computed by solving the 1D ME at 1 atm of N_2. The energies and molecular properties used in the RRKM/ME are computed with MRACPF2/CBS(D-T)//DFT-M08-HX/cc-pVTZ.

three CSEs are labeled by their magnitude. The slowest CSE $-\lambda_1$ describes reaction R1, i.e., the equilibration of $CH_2C(=O)$ + CH_3O with $CH_2C(=O)OCH_3$. The fastest ($-\lambda_3$) corresponds to the equilibration of $CH_2C(=O)$ + CH_3O and $CH_2C(=O)OCH_3$ with $CH_3C(=O)OCH_2$, while $-\lambda_2$ "equilibrates" the three configurations ($CH_2C(=O)$ + CH_3O, $CH_2C(=O)OCH_3$, and $CH_3C(=O)OCH_2$) with the bimolecular sink $CH_3C(=O)$ + HCHO. Since TS1 exhibits much higher energy than TS2 and TS3, $-\lambda_1$ is widely separated from the other CSEs in magnitude. $-\lambda_3$ merges with IEREs at ~2500 K, indicating that the dissociation of $CH_2C(=O)OCH_3$ equilibrates on the internal-energy relaxation time scales. For temperatures at which the CSEs are smaller than the IEREs, i.e., the energy relaxation processes are completed before chemical transformations become significant, phenomenological rate constants for the unimolecular reactions were computed from the eigenvalues/eigenvectors,[24,25,50] where the corresponding reactants ($CH_2C(=O)OCH_3$ or $CH_3C(=O)OCH_2$) were assumed to be Boltzmann distributed.

Figure 4 compares the predicted high-pressure-limit rate constants $k_i^{\infty}(T)$ (i = 1−3) of the three unimolecular reactions with available theoretical and estimated coefficients. The energetics are computed at the CCSD(T)/CBS(T-Q) (black solid curves) and MRACPF2/CBS(D-T) (red solid curves) level. CCSD(T) predicts slightly higher barrier heights than MRACPF2, and $k_i^{\infty}(T)$ (i = 1−3) with CCSD(T) energies are therefore smaller than with MRACPF2 energies by 7−88%. Given the relatively large multiconfigurational character of the TSs, rate coefficients with MRACPF2 energies are recommended. The high-pressure-limit rate reported by Huynh and Violi[13] (green dashed curve) was obtained using RRKM theory with the reaction energetics computed at the DFT-BH&HLYP/cc-pVTZ level, which is also plotted in Figure 4a for comparison. $k_1^{\infty}(T)$ using MRACPF2 energies is comparable with the predictions of Huynh and Violi. The high-pressure-limit rate coefficients of reactions R1 and R2 in Dagaut et al.'s[5] MA combustion model were solely approximated based on the similarity relation of structure and rate. Peukert et al.[8]

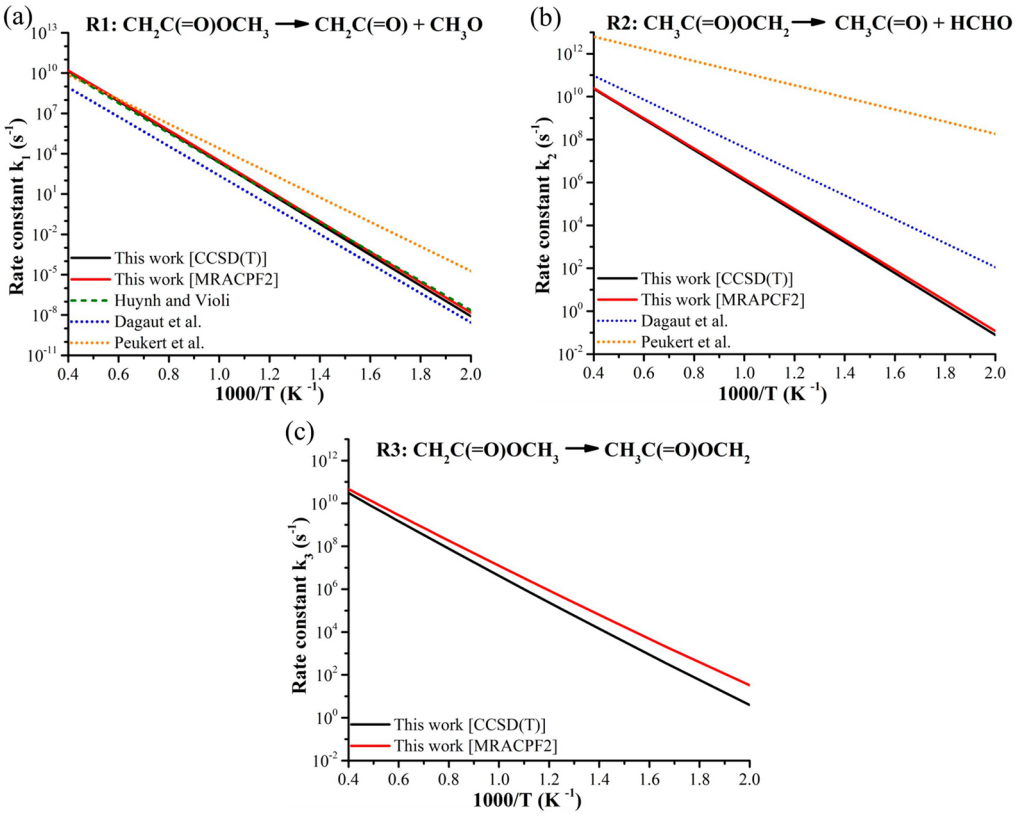

Figure 4. Comparison of the predicted high-pressure-limit rate constants $k_i^{\infty}(T)$ for Ri (i = 1−3), using energies obtained by CCSD(T)/CBS(T-Q) (black curves) and MRACPF2/CBS(D-T) (red curves), with rates derived from the modified Arrhenius expressions theoretically obtained by Huynh and Violi[13] (green dashed curves) and estimated by Dagaut et al.[5] and Peukert et al.[8]

DOI: 10.1021/acs.jpca.5b08331
J. Phys. Chem. A XXXX, XXX, XXX−XXX

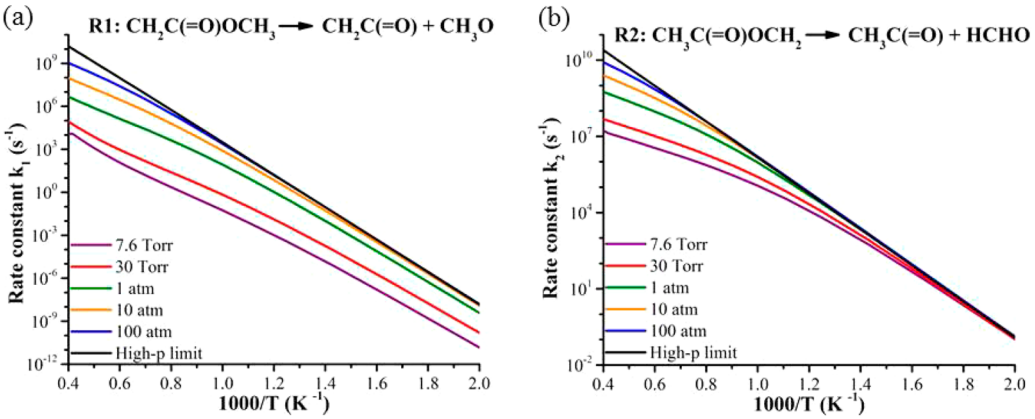

Figure 5. Comparison of predicted temperature- and pressure-dependent rate constants $k_i(T,p)$ for reactions R1 and R2 at p = 7.6 Torr, 30 Torr, 1 atm, 10 atm, 100 atm, and the high-pressure limit. The energies and molecular properties used in the RRKM/ME are computed with MRACPF2/CBS(D-T)//DFT-M08-HX/cc-pVTZ.

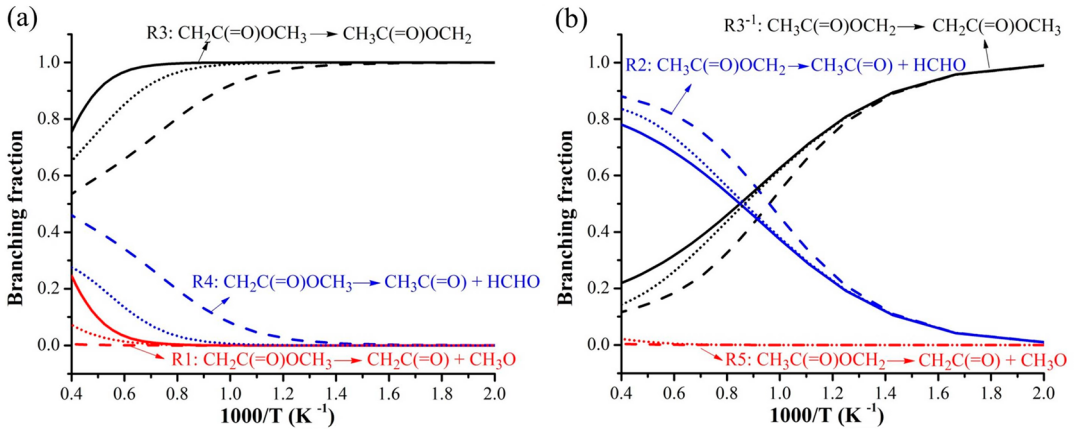

Figure 6. Comparison of the predicted branching fractions for the $CH_2C(=O)OCH_3$ and $CH_3C(=O)OCH_2$ radicals dissociating to $CH_2C(=O)$ + CH_3O (red) and $CH_3C(=O)$ + HCHO (blue), and isomerizing to the other (black) at 1 atm (dashed curves), 100 atm (dotted curves), and high-pressure limit (solid curves). The energies and molecular properties used in the RRKM/ME are computed with MRACPF2/CBS(D-T)//DFT-M08-HX/cc-pVTZ. The notation $R3^{-1}$ represents the reverse of reaction R3.

computed $k_1^{\infty}(T)$ and $k_2^{\infty}(T)$ using the rate coefficients of the backward reactions R1 and R2 estimated by Westbrook et al.[10] The two estimates differ by orders of magnitude from each other and from Huynh and Violi's and our theoretical predictions (Figure 4a and Figure 4b).

However, it is not sufficient to only consider the β-scission decomposition of $CH_2C(=O)OCH_3$ and $CH_3C(=O)OCH_2$ in the kinetics calculations. A collisionally activated $CH_2C(=O)OCH_3$ radical may isomerize to an energized $CH_3C(=O)OCH_2$ radical, which then may dissociate to $CH_3C(=O)$ + HCHO before it is thermally stabilized to $CH_3C(=O)OCH_2$ (Figure 2). This process cannot be accurately described by just combining the two reactions R2 and R3. Similarly, $CH_3C(=O)OCH_2$ can decompose to $CH_2C(=O)$ + CH_3O through isomerization step R3. This is especially important when an isomerization barrier is lower than a corresponding dissociation barrier. Consequently, in addition to the two direct β-scission reactions R1 and R2, there are two other dissociation channels R4 and R5 contributing to consumption of the two radicals, as follows:

$$CH_2C(=O)OCH_3 \rightarrow CH_3C(=O) + HCHO \quad (R4)$$

$$CH_3C(=O)OCH_2 \rightarrow CH_2C(=O) + CH_3O \quad (R5)$$

Therefore, reactions R4 and R5 should also be included in the multiwell ME calculations to obtain the correct temperature- and pressure-dependence of the rate coefficients for this reaction system. Table 1 lists fitted modified Arrhenius parameters for the five rate coefficients $k_i(T,p)$ (i = 1−5) at different pressures, with energies and molecular properties obtained at the MRACPF2/CBS(D-T)//DFT-M08-HX/cc-pVTZ level. Figure 5a and Figure 5b compare rate coefficients $k_i(T,p)$ of the two β-scission reactions R1 and R2. It is evident that the rate constants at finite pressures differ significantly from the high-pressure limits, and the deviations grow with increasing temperature. Especially, $k_1(T,p)$ at low pressures is orders of magnitude smaller than the corresponding high-pressure limit even at 500 K.

To better understand the reaction paths and product distributions, branching ratios of reactions contributing to the consumption of the two radicals are also analyzed. Figure 6a depicts the branching fractions of the $CH_2C(=O)OCH_3$ dissociation (R1 and R4) and isomerization (R3) reactions at 1 atm (dashed curves), 100 atm (dotted curves), and the high-pressure limit (solid curves), defined as $(k_i/(k_1 + k_3 + k_4))$ for each reaction Ri (i = 1,3,4). In the high-pressure limit, the computed phenomenological rate constant of each reaction coincides with the result obtained with TS theory, and

DOI: 10.1021/acs.jpca.5b08331
J. Phys. Chem. A XXXX, XXX, XXX−XXX

therefore $k_4^{\infty} \rightarrow 0$ and is not shown. Because of the high barrier height of reaction R1, less than 25% of $CH_2C(=O)OCH_3$ dissociates to the bimolecular product $CH_2C(=O) + CH_3O$, and all the rest isomerizes to the $CH_3C(=O)OCH_2$ radical. When the phenomenological rate coefficients obtained with the multiple-well ME theory are investigated at finite pressures, competition between the three reactions further intensifies the difference in the rate coefficients if obtained in a single channel calculation. Consequently, no more than 7% of $CH_2C(=O)OCH_3$ is consumed by the reaction R1 at 100 atm, which is much smaller than the high-pressure-limit ratio. As expected, the contribution of reaction R4 grows as the pressure decreases and the branching ratios for reactions R3 and R4 at 2500 K and 1 atm are about 53% and 46%, respectively. Regarding the consumption of $CH_3C(=O)OCH_2$, the contribution of reaction R5 is negligible (Figure 6b). The branching ratio of β-scission reaction R2 is smaller than that of the isomerization reaction at relatively low temperature due to its high activation energy. It increases rapidly with temperature, since the corresponding TS gains more entropy relative to the reactant than that of the isomerization reaction. Consequently, both $CH_2C(=O)OCH_3$ and $CH_3C(=O)OCH_2$ radicals mainly decompose to the bimolecular pair $CH_3C(=O)$ and HCHO eventually rather than to $CH_2C(=O) + CH_3O$. It is worth emphasizing that not only the reaction rates but also the branching fractions at finite pressures are predicted to differ significantly from the high-pressure-limit results, especially under combustion conditions. This pressure dependence suggests that incorporating the pressure-dependent rate coefficients for these unimolecular reactions is crucial to accurately describe the reaction kinetics, especially when there are competing reactions.

3.3. Implications for the MA Combustion Mechanism.

To the best of our knowledge, none of the MA combustion models developed by Dagaut et al.,[5] Westbrook et al.,[10] and Peukert et al.[8] include the pressure dependence of reactions R1 and R2 or of the channels R3, R4, and R5. These mechanisms proposed that $CH_2C(=O)OCH_3$, produced by H-abstraction of MA, completely dissociated to the bimolecular product $CH_2C(=O) + CH_3O$ under combustion conditions, which can lead to improper results. For example, Westbrook et al.[10] concluded that reaction path R1 produced all the $CH_2C(=O)$ that was observed in the low pressure flame experiment of MA oxidation, but the simulated $CH_2C(=O)$ concentrations were much larger than the experimental measurements. By contrast, in our work the dissociation reaction paths of the two radicals to $CH_2C(=O) + CH_3O$ are predicted to be minor players, and the $CH_2C(=O)OCH_3$ radical is predicted to mainly decompose to $CH_3C(=O) + HCHO$, with much higher rate coefficients than to $CH_2C(=O) + CH_3O$. Namely, both reactions R1 and R5 contribute negligibly to the formation of $CH_2C(=O)$ under combustion conditions. The observed $CH_2C(=O)$ in Westbrook et al.'s experiments must result from some other reactions, such as the MA decomposition reaction $CH_3C(=O)OCH_3 \rightarrow CH_2C(=O) + CH_3OH$, which is not included in Westbrook et al.'s model. Moreover, compared to the dissociation products $CH_2C(=O) + CH_3O$ which dissociate to $CH_2CO + HCHO + H$ at high temperatures, the products $CH_3C(=O) + HCHO$ may further break apart to form $CO + HCHO + CH_3$, producing a less active radical (CH_3) rather than an H atom. This may result in lower reactivity in MA combustion. These pathways also help explain the observation that MA/air mixtures exhibit slower kinetics than methyl formate (MF) and methyl propanoate (MP)/air mixtures, as indicated by the comparison of flame extinction limits and laminar flame speeds.[6,9] Compared to the reaction pathways of MA radicals, dominant reaction pathways for the dissociation of MF and MP radicals produced from H-abstraction resulted in more reactive intermediates with a higher production rate of H atoms.[6]

To correct these problems, a new MA combustion mechanism was constructed with updated rate coefficients for MA-related reactions. The rate coefficients used for MA decomposition are the averages of two theoretical predictions by Peukert et al.[8] and Annesley et al.[51] with a factor of 3 increase for the reaction $CH_3C(=O)OCH_3 \rightarrow CH_2C(=O) + CH_3OH$ to fit our previous flow reactor experiments.[11] Rates of MA H-abstraction by H, O, OH, HO_2, and CH_3, as well as MA radical unimolecular reactions, were computed in our previous work[12] and in the present work. The parameters for all other reactions were obtained from Shen et al.'s[52] work, referred to as the HP-Mech submodel. This new model (red solid curve) successfully simulates the recent experiments of the MA/air mixture laminar flame speed measured by Wang et al. (black squares)[9] at the initial temperature of 333 K and similarly at 338 K by Ali Hamdi Bnayan[53] (gray circles) (Figure 7). The

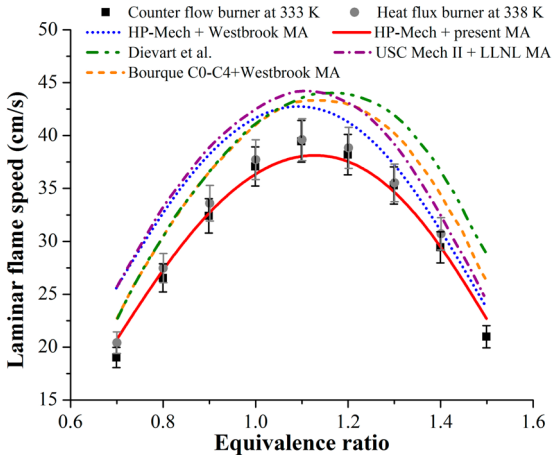

Figure 7. Comparison of computed laminar flame speed of MA/air mixtures with measured results by Wang et al. (black squares)[9] at 333 K and by Ali Hamdi Bnayan[53] (gray circles) at 338 K. The simulations are performed at 333 K with five MA combustion models: HP-Mech[52] submodel combined with MA-related reactions from Westbrook et al.'s[10] work (blue dotted curve); HP-Mech[52] submodel combined with MA-related reactions predicted in this work (red solid curve); model developed by Dievart et al.[54] (green dash dot dot curve); submodel for C0−C4 species from Bourque et al.[55] combined with MA-related reactions from Westbrook et al.'s[10] work (orange dashed curve); and submodel for C0−C4 species from USC Mech II[56] combined with MA-related reactions from Wang et al.'s[9] work (purple dash dot curve).

simulation results of a few other models,[9,10,54−56] which are commonly used to investigate MA combustion chemistry, are also plotted for comparison. For further analysis of the potential impact of the MA-related reactions, a simulation using a combination of HP-Mech submodel and MA-related reaction rates from Westbrook et al.'s[10] model is also compared in Figure 7 (blue solid curve). Our new model incorporating the theoretically predicted rate coefficients exhibits better agreement with the experiments. The comparison demonstrates

DOI: 10.1021/acs.jpca.5b08331
J. Phys. Chem. A XXXX, XXX, XXX−XXX

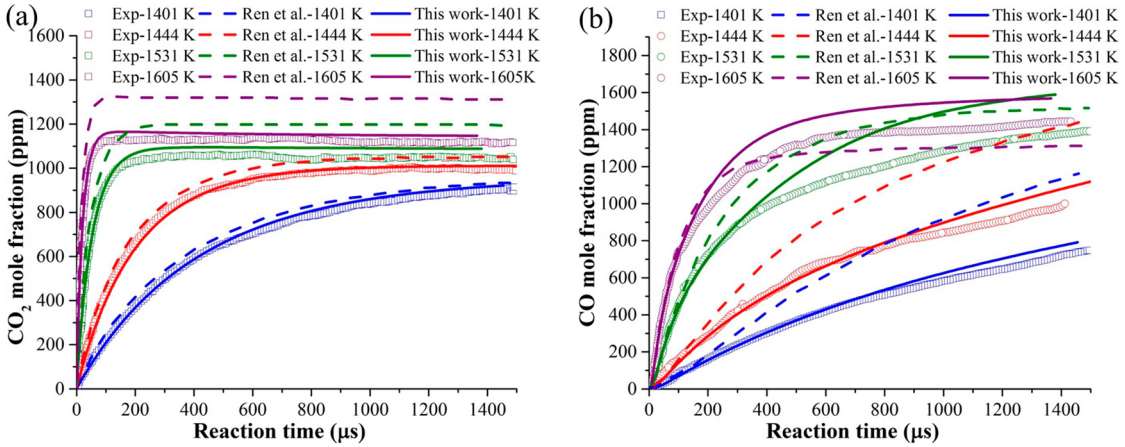

Figure 8. (a) CO_2 and (b) CO time-histories predicted using our updated model (solid curves) compared with corresponding simulations (dashed curves) and experimental results (symbols) by Ren et al.[57] at four temperatures.

the success of our theoretical predictions of rate constants for the MA-related reactions.

The new model was also validated against the most recent MA decomposition experiment using the Stanford shock tube facilities.[57] Figure 8 depicts the comparison of simulations using the current model (solid curves) and the model updated by Ren et al.[57] (dashed curves) against the measured CO and CO_2 time history profiles (symbols) at four temperatures. It is clear that our new model improves upon the predictions of Ren et al.'s[57] mechanism with regard to predicting the CO and CO_2 concentrations. The discrepancy for the plateau in CO concentration at high temperature for longer oxidation times suggests that there might be some uncertainty in the C1 submodel of the current mechanism. However, this issue may be related to reactions of CH_3OH and is therefore beyond the scope of this work. Overall, the good agreement between the simulations with our model and experimental values indicates that the rate constants and branching ratios of MA-related reactions have been well-predicted.

4. CONCLUSIONS

The unimolecular dissociation and isomerization PESs of the $CH_2C(=O)OCH_3$ and $CH_3C(=O)OCH_2$ radicals were theoretically investigated at the CCSD(T)/CBS, MRSDCI +DS/CBS, and MRACPF2/CBS levels of theory, based on the geometries of stationary points obtained at the DFT-M08-HX/cc-pVTZ level. Relatively large T1 diagnostics in CCSD(T) calculations suggested high multiconfigurational character in this reaction system, particularly at the TSs. Hence, the multireference methods, MRSDCI+DS and MRACPF2, which predicted lower barrier heights than CCSD(T), are considered to be more reliable for kinetics calculations. The isomerization reaction between the two radicals exhibits a lower activation energy than both β-scission reactions of the two radicals, indicating that the isomerization is energetically more favorable and the decomposition of the two radicals are strongly coupled at finite pressures.

RRKM and multiwell ME calculations of this reaction system show that the rate coefficients and branching fractions of each channel differed significantly from the high-pressure limits, demonstrating the importance of incorporating pressure-dependence into kinetics models for these unimolecular reactions. The dissociation of $CH_2C(=O)OCH_3$ to $CH_2C(=O)$ + CH_3O was predicted to be not important at all, contrary to previous combustion models.[5,8−10] Instead, more than 93% of $CH_2C(=O)OCH_3$ was predicted to either decompose to the bimolecular product $CH_3C(=O)$ + HCHO or isomerize to $CH_3C(=O)OCH_2$ over a wide range of temperatures and finite pressures. Likewise, the $CH_3C(=O)OCH_2$ radical was also predicted to be predominantly consumed by the isomerization reaction and the dissociation to $CH_3C(=O)$ + HCHO. The branching ratio of the β-scission reaction increased rapidly with temperature. A new MA combustion model was constructed with updates of predicted rate constants for MA-related reactions. The improved agreement between simulations and experimental results further validates the success of our predicted reaction rates.

■ ASSOCIATED CONTENT

Supporting Information

The Supporting Information is available free of charge on the ACS Publications website at DOI: 10.1021/acs.jpca.5b08331.

Coordinates of optimized geometries and vibrational frequencies for all species presented in this work at the DFT-M08-HX/cc-pVTZ level of theory, the fitted temperature- and pressure-dependent rate constants for all reactions, with CCSD(T)/CBS(T-Q) energies with the bath gas N_2 in modified Arrhenius expressions, and the modified Arrhenius parameters with the bath gas Ar (PDF)

■ AUTHOR INFORMATION

Corresponding Author

*E-mail: eac@princeton.edu. Phone: (609) 258-5391. Fax: +1 (609) 258-5877.

Notes

The authors declare no competing financial interest.

■ ACKNOWLEDGMENTS

This work was supported by the Combustion Energy Frontier Research Center funded by the U.S. Department of Energy, Office of Science, and the Office of Basic Energy Sciences under Award DE-SC0001198. X.Y. and Y.J. used resources of the National Energy Research Scientific Computing Center, a DOE Office of Science User Facility supported by the Office of Science of the U.S. Department of Energy under Contract DE-AC02-05CH11231, for some preliminary calculations.

DOI: 10.1021/acs.jpca.5b08331
J. Phys. Chem. A XXXX, XXX, XXX−XXX

REFERENCES

(1) Graboski, M. S. M.; McCormick, R. L. R. Combustion of Fat and Vegetable Oil Derived Fuels in Diesel Engines. *Prog. Energy Combust. Sci.* **1998**, *24*, 125−164.

(2) Feng, Y.; Le Doan, T. V.; Pomerantz, A. E. The Chemical Composition of Bitumen in Pyrolyzed Green River Oil Shale: Characterization by ^{13}C NMR Spectroscopy. *Energy Fuels* **2013**, *27*, 7314−7323.

(3) Kohse-Höinghaus, K.; Oßwald, P.; Cool, T. A.; Kasper, T.; Hansen, N.; Qi, F.; Westbrook, C. K.; Westmoreland, P. R. Biofuel Combustion Chemistry: From Ethanol to Biodiesel. *Angew. Chem., Int. Ed.* **2010**, *49*, 3572−3597.

(4) Lai, J. Y. W.; Lin, K. C.; Violi, A. Biodiesel Combustion: Advances in Chemical Kinetic Modeling. *Prog. Energy Combust. Sci.* **2011**, *37*, 1−14.

(5) Dagaut, P.; Smoucovit, N.; Cathonnet, M. Methyl Acetate Oxidation in a JSR: Experimental and Detailed Kinetic Modeling Study. *Combust. Sci. Technol.* **1997**, *127*, 275−291.

(6) Diévart, P.; Won, S. H.; Gong, J.; Dooley, S.; Ju, Y. A Comparative Study of the Chemical Kinetic Characteristics of Small Methyl Esters in Diffusion Flame Extinction. *Proc. Combust. Inst.* **2013**, *34*, 821−829.

(7) Osswald, P.; Struckmeier, U.; Kasper, T.; Kohse-Höinghaus, K.; Wang, J.; Cool, T. A.; Hansen, N.; Westmoreland, P. R. Isomer-Specific Fuel Destruction Pathways in Rich Flames of Methyl Acetate and Ethyl Formate and Consequences for the Combustion Chemistry of Esters. *J. Phys. Chem. A* **2007**, *111*, 4093−4101.

(8) Peukert, S. L.; Sivaramakrishnan, R.; Su, M.-C.; Michael, J. V. Experiment and Theory on Methylformate and Methylacetate Kinetics at High Temperatures: Rate Constants for H-Atom Abstraction and Thermal Decomposition. *Combust. Flame* **2012**, *159*, 2312−2323.

(9) Wang, Y. L.; Lee, D. J.; Westbrook, C. K.; Egolfopoulos, F. N.; Tsotsis, T. T. Oxidation of Small Alkyl Esters in Flames. *Combust. Flame* **2014**, *161*, 810−817.

(10) Westbrook, C. K.; Pitz, W. J.; Westmoreland, P. R.; Dryer, F. L.; Chaos, M.; Osswald, P.; Kohse-Höinghaus, K.; Cool, T. a.; Wang, J.; Yang, B.; et al. A Detailed Chemical Kinetic Reaction Mechanism for Oxidation of Four Small Alkyl Esters in Laminar Premixed Flames. *Proc. Combust. Inst.* **2009**, *32*, 221−228.

(11) Yang, X.; Felsmann, D.; Kurimoto, N.; Krüger, J.; Wada, T.; Tan, T.; Carter, E. A.; Kohse-Höinghaus, K.; Ju, Y. Kinetic Studies of Methyl Acetate Pyrolysis and Oxidation in a Flow Reactor and a Low-Pressure Flat Flame Using Molecular-Beam Mass Spectrometry. *Proc. Combust. Inst.* **2015**, *35*, 491−498.

(12) Tan, T.; Yang, X.; Krauter, C. M.; Ju, Y.; Carter, E. A. Ab Initio Kinetics of Hydrogen Abstraction from Methyl Acetate by Hydrogen, Methyl, Oxygen, Hydroxyl, and Hydroperoxy Radicals. *J. Phys. Chem. A* **2015**, *119*, 6377−6390.

(13) Huynh, L. K.; Lin, K. C.; Violi, A. Kinetic Modeling of Methyl Butanoate in Shock Tube. *J. Phys. Chem. A* **2008**, *112*, 13470−13480.

(14) Kohn, W.; Sham, L. J. Self-Consistent Equations Including Exchange and Correlation Effects. *Phys. Rev.* **1965**, *140*, 1133−1138.

(15) Rice, O. K.; Ramsperger, H. C. Theories of Unimolecular Gas Reactions at Low Pressures. *J. Am. Chem. Soc.* **1927**, *49*, 1617−1629.

(16) Kassel, L. S. Studies in Homogeneous Gas Reactions. I. *J. Phys. Chem.* **1928**, *32*, 225−242.

(17) Marcus, R. A. Unimolecular Dissociations and Free Radical Recombination Reactions. *J. Chem. Phys.* **1952**, *20*, 359−364.

(18) Zhao, L.; Xie, M.; Ye, L.; Cheng, Z.; Cai, J.; Li, Y.; Qi, F.; Zhang, L. An Experimental and Modeling Study of Methyl Propanoate Pyrolysis at Low Pressure. *Combust. Flame* **2013**, *160*, 1958−1966.

(19) Raghavachari, K.; Trucks, G. W.; Pople, J. A.; Head-Gordon, M. A Fifth-Order Perturbation Comparison of Electron Correlation Theories. *Chem. Phys. Lett.* **1989**, *157*, 479−483.

(20) Siegbahn, P. E. M. Generalizations of the Direct CI Method Based on the Graphical Unitary Group Approach. II. Single and Double Replacements from Any Set of Reference Configurations. *J. Chem. Phys.* **1980**, *72*, 1647.

(21) Davidson, E. R.; Silver, D. W. Size Consistency in the Dilute Helium Gas Electronic Structure. *Chem. Phys. Lett.* **1977**, *52*, 403−406.

(22) Gdanitz, R. J.; Ahlrichs, R. The Averaged Coupled-Pair Functional (ACPF): A Size-Extensive Modification of MR CI(SD). *Chem. Phys. Lett.* **1988**, *143*, 413−420.

(23) Gdanitz, R. J. A New Version of the Multireference Averaged Coupled-Pair Functional (MR-ACPF-2). *Int. J. Quantum Chem.* **2001**, *85*, 281−300.

(24) Klippenstein, S. J.; Miller, J. A. From the Time-Dependent, Multiple-Well Master Equation to Phenomenological Rate Coefficients. *J. Phys. Chem. A* **2002**, *106*, 9267−9277.

(25) Miller, J. A.; Klippenstein, S. J. The Recombination of Propargyl Radicals: Solving the Master Equation. *J. Phys. Chem. A* **2001**, *105*, 7254−7266.

(26) Zhao, Y.; Truhlar, D. G. Exploring the Limit of Accuracy of the Global Hybrid Meta Density Functional for Main-Group Thermochemistry, Kinetics, and Noncovalent Interactions. *J. Chem. Theory Comput.* **2008**, *4*, 1849−1868.

(27) Dunning, T. H. Gaussian Basis Sets for Use in Correlated Molecular Calculations. I. The Atoms Boron through Neon and Hydrogen. *J. Chem. Phys.* **1989**, *90*, 1007.

(28) Gordon, M. S.; Schmidt, M. W. Advances in Electronic Structure Theory: GAMESS a Decade Later. In *Theory and Applications of Computational Chemistry: The First Forty Years*; Elsevier: Amsterdam, 2005; pp 1167−1189.

(29) Alecu, I. M.; Zheng, J.; Zhao, Y.; Truhlar, D. G. Computational Thermochemistry: Scale Factor Databases and Scale Factors for Vibrational Frequencies Obtained from Electronic Model Chemistries. *J. Chem. Theory Comput.* **2010**, *6*, 2872−2887.

(30) Werner, H.-J.; Knowles, P. J.; Knizia, G.; Manby, F. R.; Schütz, M. Molpro: A General-Purpose Quantum Chemistry Program Package. *WIREs Comput. Mol. Sci.* **2012**, *2*, 242−253.

(31) Aquilante, F.; De Vico, L.; Ferré, N.; Ghigo, G.; Malmqvist, P.-å.; Neogrády, P.; Pedersen, T. B.; Pitoňák, M.; Reiher, M.; Roos, B. O.; Serrano-Andrés, L.; Urban, M.; Veryazov, V.; Lindh, R. MOLCAS 7: The Next Generation. *J. Comput. Chem.* **2010**, *31*, 224−247.

(32) Walter, D.; Carter, E. A. Multi-Reference Weak Pairs Local Configuration Interaction: Efficient Calculations of Bond Breaking. *Chem. Phys. Lett.* **2001**, *346*, 177−185.

(33) Walter, D.; Venkatnathan, A.; Carter, E. A. Local Correlation in the Virtual Space in Multireference Singles and Double Configuration Interaction. *J. Chem. Phys.* **2003**, *118*, 8127−8139.

(34) Chwee, T. S.; Szilva, A. B.; Lindh, R.; Carter, E. A. Linear Scaling Multireference Singles and Doubles Configuration Interaction. *J. Chem. Phys.* **2008**, *128*, 224106.

(35) Chwee, T. S.; Carter, E. A. Cholesky Decomposition within Local Multireference Singles and Doubles Configuration Interaction. *J. Chem. Phys.* **2010**, *132*, 074104.

(36) Krisiloff, D. B.; Carter, E. A. Approximately Size Extensive Local Multireference Singles and Doubles Configuration Interaction. *Phys. Chem. Chem. Phys.* **2012**, *14*, 7710−7717.

(37) Krisiloff, D. B.; Oyeyemi, V. B.; Libisch, F.; Carter, E. A. Analysis of and Remedies for Unphysical Ground States of the Multireference Averaged Coupled-Pair Functional. *J. Chem. Phys.* **2014**, *140*, 024102.

(38) Dieterich, J. M.; Krisiloff, D. B.; Gaenko, A.; Libisch, F.; Windus, T. L.; Gordon, M. S.; Carter, E. A. Shared-Memory Parallelization of a Local Correlation Multi-Reference CI Program. *Comput. Phys. Commun.* **2014**, *185*, 3175−3188.

(39) Krisiloff, D. B.; Dieterich, J. M.; Libisch, F.; Carter, E. A. Numerical Challenges in a Cholesky-Decomposed Local Correlation Quantum Chemistry Framework. In *Mathematical and Computational Modeling with Applications in Engineering and the Natural and Social Sciences*; Melnik, R., Ed.; Wiley: Hoboken, NJ, 2015.

(40) Dieterich, J. M.; Carter, E. A. Assessment of a Semi Integral-Direct Local Multi-Reference Configuration Interaction Implementation Employing Shared-Memory Parallelization. *Comput. Theor. Chem.* **2015**, *1051*, 47−56.

DOI: 10.1021/acs.jpca.5b08331
J. Phys. Chem. A XXXX, XXX, XXX−XXX

(41) Feller, D.; Dixon, D. A. Extended Benchmark Studies of Coupled Cluster Theory through Triple Excitations. *J. Chem. Phys.* **2001**, *115*, 3484.
(42) Klippenstein, S. J.; Wagner, A. F.; Dunbar, R. C.; Wardlaw, D. M.; Robertson, S. H.; Miller, J. A. *VariFlex*; Argonne National Laboratory: Argonne, IL, 2003.
(43) Tan, T.; Pavone, M.; Krisiloff, D. B.; Carter, E. A. Ab Initio Reaction Kinetics of Hydrogen Abstraction from Methyl Formate by Hydrogen, Methyl, Oxygen, Hydroxyl, and Hydroperoxy Radicals. *J. Phys. Chem. A* **2012**, *116*, 8431−8443.
(44) Poling, B. E.; Prausnitz, J. M.; O'Connell, J. P. *Properties of Gases and Liquids*; McGraw-Hill: New York, 2001
(45) Johnston, S.; Heicklen, J. Tunnelling Corrections For Unsymmetrical Eckart Potential Energy Barriers. *J. Phys. Chem.* **1962**, *66*, 532−533.
(46) Lee, T. J.; Taylor, P. R. A Diagnostic for Determining the Quality of Single-Reference Electron Correlation Methods. *Int. J. Quantum Chem.* **1989**, *36*, 199−207.
(47) Taylor, P. R. Coupled-Cluster Methods in Quantum Chemistry. In *Lecture Notes in Quantum Chemistry II*; Roos, B. O., Ed.; Springer-Verlag: Berlin, 1994.
(48) Szalay, P. G. Configuration Interaction: Corrections for Size-Consistency. In *Encyclopedia of Computational Chemistry*; John Wiley & Sons, Ltd.: Chichester, U.K., 2005.
(49) Goos, E.; Burcat, A.; Ruscic, B. Extended Third Millennium Ideal Gas and Condensed Phase Thermochemical Database for Combustion with Updates from Active Thermochemical Tables. Report TAE960; Office of Scientific and Technical Information, U.S. Department of Energy: Oak Ridge, TN, 2013.
(50) Miller, J. A.; Klippenstein, S. J. Master Equation Methods in Gas Phase Chemical Kinetics. *J. Phys. Chem. A* **2006**, *110*, 10528−10544.
(51) Annesley, C. J.; Franklin Goldsmith, C.; Tranter, R. S. A Shock Tube Laser Schlieren Study of Methyl Acetate Dissociation in the Fall-off Regime. *Phys. Chem. Chem. Phys.* **2014**, *16*, 7241.
(52) Shen, X.; Yang, X.; Santner, J.; Sun, J.; Ju, Y. Experimental and Kinetic Studies of Acetylene Flames at Elevated Pressures. *Proc. Combust. Inst.* **2015**, *35*, 721−728.
(53) Ali Hamdi Bnayan, A. The Potential of Esters as Renewable Fuels: Determination of Laminar Burning Velocities. Masters Thesis, Lund University, Lund,Sweden, 2013.
(54) Diévart, P.; Won, S. H.; Gong, J.; Dooley, S.; Ju, Y. A Comparative Study of the Chemical Kinetic Characteristics of Small Methyl Esters in Diffusion Flame Extinction. *Proc. Combust. Inst.* **2013**, *34*, 821−829.
(55) Bourque, G.; Healy, D.; Curran, H.; Zinner, C.; Kalitan, D.; de Vries, J.; Aul, C.; Petersen, E. Ignition and Flame Speed Kinetics of Two Natural Gas Blends with High Levels of Heavier Hydrocarbons. In *Combustion, Fuels and Emissions, Parts A and B*; ASME; New York, 2008; Vol. 3, pp 1051−1066.
(56) Wang, H.; You, X.; Joshi, A. V.; Davis, S. G.; Laskin, A.; Egolfopoulos, F. N.; Law, C. K. High-Temperature Combustion Reaction Model of H_2/CO/C1-C4 Compounds. USC Mech Version II. http://ignis.usc.edu/USC_Mech_II.htm, May 2007.
(57) Ren, W. Private communication, 2015.

DOI: 10.1021/acs.jpca.5b08331
J. Phys. Chem. A XXXX, XXX, XXX−XXX